Golgi- and Trans-Golgi Network-Mediated Vesicle Trafficking Is Required for Wax Secretion from Epidermal Cells[1][W][OPEN]

Heather E. McFarlane[2], Yoichiro Watanabe, Weili Yang, Yan Huang, John Ohlrogge, and A. Lacey Samuels*

Department of Botany (H.E.M., Y.W., Y.H., A.L.S.) and Michael Smith Laboratories (Y.H.), University of British Columbia, Vancouver, British Columbia, Canada V6T 1Z4; and Department of Plant Biology, Michigan State University, East Lansing, Michigan 48824 (W.Y., J.O.)

Lipid secretion from epidermal cells to the plant surface is essential to create the protective plant cuticle. Cuticular waxes are unusual secretory products, consisting of a variety of highly hydrophobic compounds including saturated very-long-chain alkanes, ketones, and alcohols. These compounds are synthesized in the endoplasmic reticulum (ER) but must be trafficked to the plasma membrane for export by ATP-binding cassette transporters. To test the hypothesis that wax components are trafficked via the endomembrane system and packaged in Golgi-derived secretory vesicles, Arabidopsis (*Arabidopsis thaliana*) stem wax secretion was assayed in a series of vesicle-trafficking mutants, including *gnom like1-1* (*gnl1-1*), *transport particle protein subunit120-4*, and *echidna* (*ech*). Wax secretion was dependent upon GNL1 and ECH. Independent of secretion phenotypes, mutants with altered ER morphology also had decreased wax biosynthesis phenotypes, implying that the biosynthetic capacity of the ER is closely related to its structure. These results provide genetic evidence that wax export requires GNL1- and ECH-dependent endomembrane vesicle trafficking to deliver cargo to plasma membrane-localized ATP-binding cassette transporters.

The aerial, nonwoody tissues of all land plants are covered by a waxy cuticle that protects the plant against nonstomatal water loss. The cuticle also provides the first barrier between the plant and its environment and mediates important biotic and abiotic interactions. The cuticle has two main components: cutin and waxes. Cutin is a tough, cross-linked polyester matrix primarily composed of C16 and C18 oxygenated fatty acids and glycerol (Pollard et al., 2008). Wax is a heterogenous mixture, primarily composed of very-long-chain (VLC) fatty acid derivatives (predominantly 29-carbon alkane in Arabidopsis [*Arabidopsis thaliana*] stems).

As a result of biochemical approaches, forward genetic screens yielding the *eceriferum* (*cer*) mutants (Koornneef et al., 1989), and reverse genetics approaches (Greer et al., 2007), almost all of the enzymes in the wax biosynthesis pathway have been identified. The enzymes that elongate C16 or C18 fatty acids to VLC (greater than 20C) fatty acids are localized in the endoplasmic reticulum (ER; for review, see Haslam and Kunst, 2013). Primary alcohols are synthesized by the fatty acyl reductases (Rowland et al., 2006), while alkanes are generated via an undefined mechanism involving CER1, CER3, and an unidentified cytochrome b_5 (Bernard et al., 2012). These alkanes may be modified by the midchain alkane hydroxylase cytochrome P450 (MAH1) to generate secondary alcohols and ketones (Greer et al., 2007). All of these wax synthesis enzymes have also been localized to the ER (Greer et al., 2007; Bernard et al., 2012).

In contrast to wax synthesis, comparatively little is known about how waxes are trafficked within the cell from their site of synthesis at the ER to the plasma membrane. ATP-binding cassette (ABC) transporters of the G subfamily are required for wax export, and when either half-transporter is disrupted, waxes accumulate in the ER (McFarlane et al., 2010). Two extracellular glycosylphosphatidylinositol-anchored lipid transfer proteins (LTPs) are further required for wax accumulation on the plant surface (DeBono et al., 2009; Kim et al., 2012). Although these components of the molecular machinery of wax transport at the plasma membrane have been identified, the intracellular mechanisms by which waxes are transported to the plasma membrane remain undefined.

Several mechanisms have been hypothesized for the transport of waxes from the ER to the plasma membrane (for review, see Samuels et al., 2008). Waxes could be incorporated into vesicles at the ER, travel to and through the Golgi apparatus and the trans-Golgi network (TGN), and then move to the plasma membrane via vesicle secretion. These vesicles could carry

[1] This work was supported by the Natural Sciences and Engineering Research Council of Canada (Discovery grant to A.L.S. and CGS–D3 to H.E.M.).

[2] Present address: Max Planck Institute for Molecular Plant Physiology, 14476 Potsdam, Germany.

* Address correspondence to lsamuels@mail.ubc.ca.

The author responsible for distribution of materials integral to the findings presented in this article in accordance with the policy described in the Instructions for Authors (www.plantphysiol.org) is: A. Lacey Samuels (lsamuels@mail.ubc.ca).

[W] The online version of this article contains Web-only data.

[OPEN] Articles can be viewed online without a subscription.

www.plantphysiol.org/cgi/doi/10.1104/pp.113.234583

 © 2014 American Society of Plant Biologists. All Rights Reserved.

wax components within their membranes, as computational modeling of wax components in lipid bilayers indicates that VLC alkanes partition entirely into the hydrophobic phase of the bilayer (Coll et al., 2007). Alternatively, lipoproteins may bind to lipid molecules in order to solubilize them so that they can be transported as cargo in the vesicle lumen, by analogy to mammalian systems where lipoproteins are secreted from hepatocytes into the circulatory system by exocytosis via post-Golgi vesicles (for review, see Mansbach and Siddiqi, 2010). However, no analogous lipid-binding apoproteins or transport vesicles have been found in plants. It is also possible that LTPs in membrane contact sites between the ER and the plasma membrane could transfer cuticular lipids directly from the ER to the plasma membrane. However, although these membrane contact sites have been observed in plant cells (Samuels and McFarlane, 2012), no structural or functional components of membrane contact sites are known.

Early studies of VLC fatty acid trafficking used pulse-chase labeling to show that treatment with monensin, a post-Golgi trafficking inhibitor, results in decreased VLC fatty acid trafficking to the plasma membrane and a corresponding increase in these lipids in the Golgi apparatus (Bertho et al., 1991), suggesting a Golgi-dependent mechanism of VLC lipid trafficking to the plasma membrane. However, the "Golgi" fraction in this study contained significant elongase activity, which has subsequently been localized to the ER, making interpretation of these data difficult. While a variety of inhibitors are available that disrupt different stages in the secretory pathway (Zhang et al., 1993; Robinson et al., 2008), inhibitor studies of wax trafficking have proven ineffective, since the wax-producing epidermal cells do not effectively take up solutions carrying these inhibitors. This illustrates the difficulties of studying the transport of highly hydrophobic cargo, such as wax, within the single cell layer of epidermis.

The objective of this study was to determine the intracellular trafficking mechanisms underlying cuticular wax transport from the ER to the plasma membrane. Arabidopsis mutants, which have been successfully applied in wax biosynthesis studies, were used to investigate wax secretion. Well-characterized mutants with defects in vesicle traffic and protein secretion were chosen to test the hypothesis that wax components are trafficked via endomembrane vesicles. These mutant analyses indicate that wax movement from the ER to the plasma membrane requires vesicle traffic at both the ER-Golgi interface and the TGN. Independent of secretion phenotypes, strong decreases in wax synthesis were observed in mutants with altered ER morphology, which implies that ER structure influences its biosynthetic capacity for wax production.

RESULTS

Secretion Mutants Display Defects in Cuticular Wax Load on the Plant Surface

To investigate the route by which cuticular waxes are transported to the cell surface, a number of mutants with characterized defects in protein and polysaccharide trafficking at different points in the secretory pathway were tested for wax deficiency, including *gnom like1-1* (*gnl1-1*; Richter et al., 2007; Teh and Moore, 2007), *transport particle protein subunit120-4* (*trs120-4*; Qi et al., 2011), and *echidna* (*ech*; Gendre et al., 2011). *gnl1-1* are null mutants that are defective in an ADP-ribosylation factor guanine nucleotide-exchange factor, which is required for COAT PROTEIN I (COPI) vesicle formation in retrograde traffic from the Golgi apparatus to the ER (Richter et al., 2007; Teh and Moore, 2007). Both *ech* and *trs120-4* are defective in TGN protein complexes. ECH is a part of the ECH/Ypt/Rab-interacting protein complex, which is required specifically for the trafficking of secretory vesicles from the TGN to the plasma membrane (Gendre et al., 2011; Boutté et al., 2013; McFarlane et al., 2013). *ech* is a null allele (Gendre et al., 2011), while null alleles of *trs120* (*trs120-2* and *trs120-3*) are seedling lethal (Thellmann et al., 2010; Qi et al., 2011); therefore, experiments on mature plants required use of the weaker allele, *trs120-4*. TRS120 is part of the transport protein particle II (TRAPP II) large GTPase complex, which is required for secretion to the cell wall and cell plate (Thellmann et al., 2010; Qi et al., 2011). All of these mutants display cell elongation defects that result in reduced plant growth (Richter et al., 2007; Teh and Moore, 2007; Thellmann et al., 2010; Gendre et al., 2011; Qi et al., 2011), reflecting the importance of vesicle traffic in growth and cell wall production.

These trafficking mutants have been studied in a variety of experimental systems but not in a tissue with high lipid export. The stem epidermis of Arabidopsis is highly active in wax synthesis, and more than half of its acyl lipids are exported to the cuticle (Suh et al., 2005). To ensure that the phenotypes of trafficking defects in stem epidermal cells were consistent with those previously reported in seedlings, a secreted form of GFP (sec-GFP) was used as a qualitative secretion assay, confirming that these phenotypes are conserved in Arabidopsis stem epidermal cells (Supplemental Fig. S1; Batoko et al., 2000).

If wax components are transported via the secretory pathway, then a decrease in cuticular waxes is predicted in these vesicle-trafficking mutants. Examination of wild-type and mutant stems using cryo-scanning electron microscopy revealed a drastic reduction in stem wax crystals on *ech* mutant stems relative to the wild type, a moderate reduction in *gnl1-1*, and no observable reduction in *trs120-4* (Fig. 1). To quantify these changes in cuticular wax accumulation, stem surface waxes were analyzed using gas chromatography (GC) coupled to flame ionization detection (FID). Compared with wild-type stem wax loads, wax was significantly reduced in two of the vesicle-trafficking mutants, *gnl1-1* and *ech* ($P < 0.0001$, Student's t test; Table I). However, wax loads were not significantly different between the wild type and *trs120-4* mutants ($P = 0.3367$, Student's t test). Given that *trs120-4* is not a null mutant, it is possible that a wax phenotype might be observed in a stronger allele of *trs120*. However, since knockout

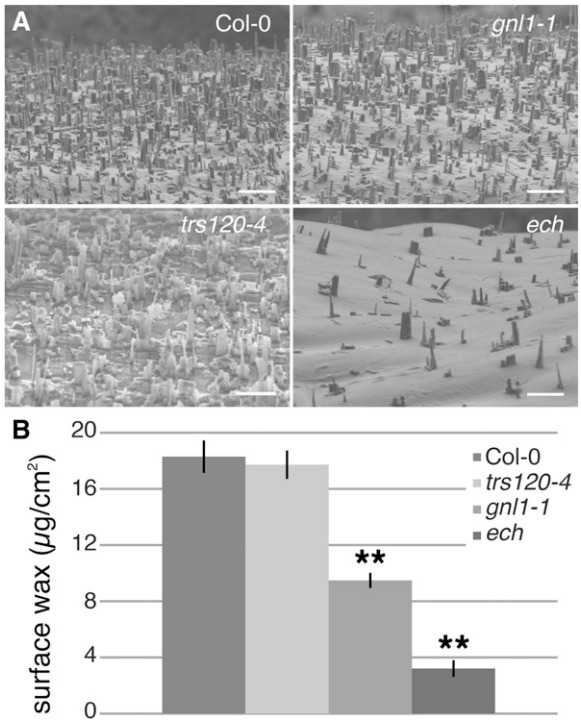

Figure 1. *gnl1-1* and *ech*, but not *trs120-4*, are defective in wax accumulation on the cell surface. A, Cryo-scanning electron microscopy of mature stems reveals dense wax crystals on wild-type and *trs120-4* stems, while *gnl1-1* and *ech* mutants have reduced wax crystals. Bars = 5 μm. B, Quantification of surface wax load via GC-FID reveals a significant decrease in surface waxes in *gnl1-1* and *ech*, but not *trs120-4*, relative to the wild type. Values are means of three experiments of three biological replicates each (i.e. $n = 9$); error bars represent SE, and asterisks indicate statistically significant differences between the wild type and the mutant (Student's *t* test, $^{**}P < 0.01$).

alleles are seedling lethal (Thellmann et al., 2010; Qi et al., 2011), their analysis was not possible. Together, these results reveal that of the three mutants that are defective in protein secretion, two mutants, *gnl1-1* and *ech*, also have strong reductions in wax accumulation on the cell surface, suggesting that wax is secreted to the plasma membrane via a Golgi-dependent mechanism that requires both GNL1 and ECH.

As wax export from the plasma membrane is dependent upon ABCG transporters, specifically ABCG11 and ABCG12, it is possible that defects in surface wax accumulation in *ech* and *gnl1-1* are caused by the mislocalization of these transporters in the vesicle-trafficking mutants. To test this, fluorescently tagged ABCG11 and ABCG12 were crossed into *gnl1-1* and *ech*. ABCG11 and ABCG12 signals at the plasma membrane were not significantly different in *ech* or *gnl1-1* stem epidermal cells compared with the wild type (Fig. 2; Supplemental Fig. S2). Additionally, if loss of ABC transporters was responsible for the wax phenotypes of *gnl1-1* and *ech*, then the chemical profiles of the vesicle-trafficking mutants would be predicted to be similar to previously described wax transport mutants (*abcg11*, *abcg12*, *ltpg1*, and *ltpg2*), which are primarily defective in alkane export (Pighin et al., 2004; Bird et al., 2007; DeBono et al., 2009; Kim et al., 2012). In contrast, *gnl1-1* and *ech* mutants were preferentially defective in the accumulation of midchain oxygenated secondary alcohols and ketones (Fig. 3; Supplemental Table S1). Together, these data indicate that the wax accumulation defects in *gnl1-1* and *ech* are not due to mislocalization of the known wax export machinery in these mutants.

The chemical profiles of the waxes that accumulate on *gnl1-1* and *ech* stems were altered compared with the wild type (Fig. 3). Specifically, *gnl1-1* and *ech* both accumulated fewer secondary alcohols and ketones (i.e. MAH1 products; Greer et al., 2007) and fewer exceptionally long-chain waxes (compounds greater than 26 carbons long [i.e. CER2 products]; Haslam et al., 2012) relative to the wild-type wax profile (Fig. 3; Supplemental Table S1). These results suggest the hypothesis that GNL1 and ECH could be preferentially required for the secretion of midchain oxygenated compounds and exceptionally long-chain waxes. However, increasing alkane levels and reducing midchain oxygenated compounds by introducing the *mah1-1* mutation into *gnl1-1* and *ech* did not significantly rescue the total wax defect of these mutants (Supplemental Fig. S3). This suggests that the preferential decrease in some wax compounds in *gnl1-1* and *ech* mutants is not the result of preferential trafficking of these components.

gnl1-1 and *ech* Mutants Are Defective in Wax Secretion

Because of the secretion defect in *gnl1-1* and *ech* mutants, we predicted that waxes that are synthesized

Table I. *Cuticular wax extracted from the plant surface compared with total stem wax in vesicle-trafficking mutants of Arabidopsis*
Average wax content (μg cm^{-2}) ± SE is shown for *trs120-4*, *rhd3-1*, *gnl1-1*, and *ech* compared with the Col-0 wild type.

Parameter	Col-0	*trs120-4*	*gnl1-1*	*ech*	*rhd3-1*
Total wax	19.8 ± 1.7	19.1 ± 1.3	12.3 ± 1.1[a,b]	6.2 ± 0.6[a,c]	8.3 ± 0.8[a]
Surface wax	18.3 ± 1.2	17.7 ± 1.0	9.5 ± 0.5[a]	3.2 ± 0.6[a]	7.4 ± 1.6[a]
Intracellular wax[d]	1.5	1.4	2.8	3.0	0.9
Percent secreted	92	93	77	52	89

[a]Statistically significant difference between the mutant and the wild type (Student's *t* test, $P < 0.01$). [b]Statistically significant difference between surface wax and total wax within a genotype (Student's *t* test, $P < 0.05$). [c]Statistically significant difference between surface wax and total wax within a genotype (Student's *t* test, $P < 0.01$). [d]Calculated from average total wax – average surface wax (μg cm^{-2}).

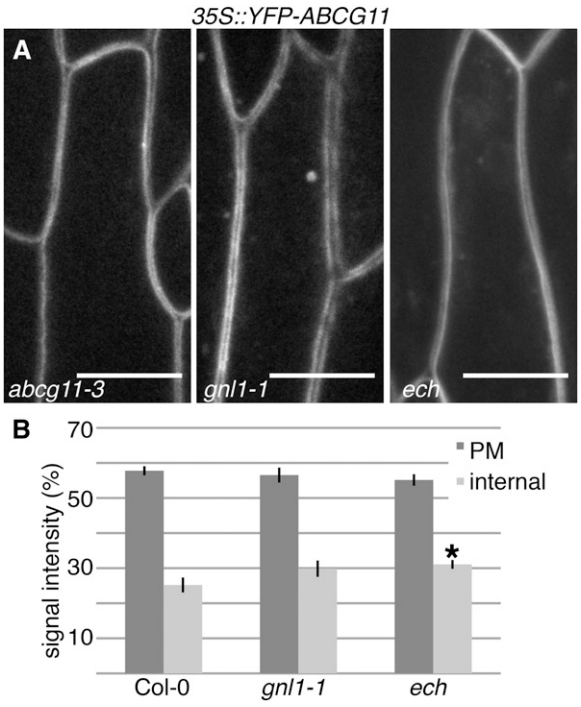

Figure 2. ABCG11 is correctly localized to the plasma membrane in *gnl1-1* and *ech*. A, In *abcg11-3* stem epidermal cells complemented with YFP-ACBG11, the transporter is localized to the plasma membrane. Despite their secretion defects, the majority of the YFP-ABCG11 signal is localized to the plasma membrane in *gnl1-1* and *ech* mutants. Bars = 10 μm. B, Quantification of the relative mean signal intensity of YFP-ABCG11 confirms no significant decrease in the localization of YFP-ABCG11 in *gnl1-1* and *ech* mutants at the plasma membrane (PM) relative to the wild type. However, *ech* mutants do accumulate significantly more internal signal than the wild type. Values are means from 18 individual cells (i.e. $n = 18$); error bars represent SE, and the asterisk indicates a statistically significant difference between the wild type and the mutant (Student's t test, $^*P < 0.05$).

but not secreted in these mutants would accumulate in the endomembrane system. The analyses of surface waxes described above were obtained by dipping stems briefly in chloroform. Internal lipids are not significantly extracted by this procedure. To quantify wax components that are not secreted, but instead accumulated within the cell, stems were homogenized in chloroform to release both surface and intracellular waxes (Table I; Supplemental Table S1). The wax profile of the ground stems compared with surface waxes was very similar; however, more components generally considered intermediates, such as fatty acids, were enriched in the ground stems (Supplemental Table S1). This is consistent with the idea that the total wax values represent the surface wax plus intracellular intermediates and wax in the process of secretion. Since surface wax extraction and total wax analysis could not be done on the same plant, plants grown together in the same pots were randomly separated into pools that were extracted for either total wax analysis or surface wax analysis, in three independent experiments. Subtracting the secreted wax value (the chloroform dip) from the total value (ground stem) provided an estimate of the quantity of wax that is retained inside the cells and/or is in the process of synthesis and secretion (Table I). In wild-type plants, the surface and total wax values were very similar (Table I), indicating that very little intracellular wax is present. By contrast, in both *ech* and *gnl1-1*, the values for total wax were significantly greater than surface wax, suggesting that in these mutants approximately 20% (*gnl1-1*) and 50% (*ech*) of the total wax that was synthesized was not secreted and accumulated inside cells (Table I).

Since the different mutants synthesize different levels of total waxes, the ratio of the wax secreted to the cuticle to the total wax synthesized was used to compare the wild type and the vesicle-trafficking mutants (Fig. 4). In wild-type stems, wax on the plant surface represented almost 93% of the total wax present in ground stems, suggesting that, at this moment in time, epidermal cells contained an intracellular pool of less than 8% of the total wax. This presumably represents waxes that are in the process of being synthesized and secreted. In *gnl1-1* mutant stems, the amount of secreted wax to total wax was reduced to almost 77%, indicating that waxes were retained inside *gnl1-1* cells and not secreted due to the vesicle-trafficking defect in these mutants. In *ech* mutants, which are defective in post-Golgi trafficking, less than 52% of the total wax was present at the cuticle, implying increased wax retention inside stem epidermal cells relative to the wild type. While ectopic deposits of extracellular lipids were occasionally observed in *ech* epidermal cells (Supplemental Fig. S4), it is expected that these apoplastic lipids would be extracted in the chloroform dip for surface lipids. As a negative control, *root hair defective3-1* (*rhd3-1*) mutants were also examined. These mutants are defective in an ER-shaping protein that is closely related to the Atlastin proteins in humans and a yeast (*Saccharomyces cerevisiae*) homolog; *rhd3-1* mutants have defects in ER morphology but not secretion (Chen et al., 2011). Although *rhd3-1* is a point mutant, it produces no detectable RHD3 protein (Zhang et al., 2013). The ratio of wax on the *rhd3-1* plant surface relative to total wax in *rhd3-1* ground stems was similar to that in the wild type, demonstrating that *rhd3-1* mutants are not defective in wax secretion. Thus, in contrast to *rhd3-1*, where secretion is not impaired, the decreased ratio of surface wax to total wax in the vesicle-trafficking mutants *gnl1* and *ech* indicates a role for GNL1- and ECH-mediated vesicle trafficking in the export of cuticular lipids.

Surface Wax Components Are Associated with Intracellular Membranes

Computational modeling has predicted that cuticular waxes will partition into the hydrophobic phase of a lipid bilayer (Coll et al., 2007). Thus, if waxes are

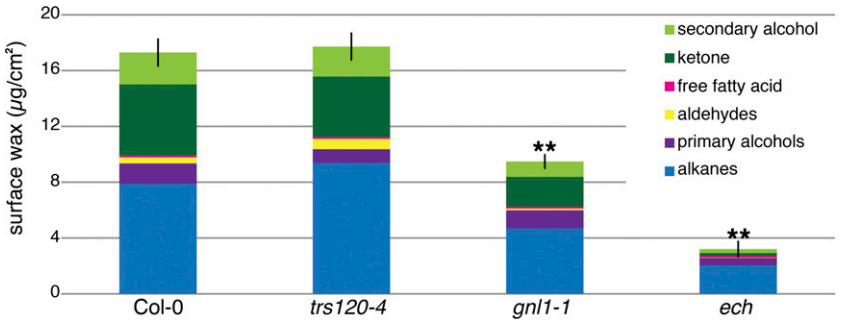

Figure 3. Wax composition is altered in *gnl1-1* and *ech*, but not *trs120-4*, mutants. Quantification of cuticular wax using GC-FID reveals a significant overall change to the composition of surface waxes in *gnl1-1* and *ech*, but not in *trs120-4*, relative to the wild type. In particular, *gnl1-1* and *ech* have decreased levels of ketones and secondary alcohols (MAH1 products; green) relative to alkanes (blue). Values are means of three experiments of three biological replicates each (i.e. $n = 9$); error bars represent SE of total surface wax load, and asterisks indicate statistically significant differences between the wild type and the mutant (Student's *t* test, $^{**}P < 0.01$).

transported via vesicle trafficking, cuticular lipids should be detected in the endomembrane system. To examine the distribution of wax components in intracellular membranes, ER-rich microsomes and ER-depleted mitochondrial fractions were isolated and analyzed by GC-mass spectrometry (MS). Unexpectedly, C29 alkane, the major component of Arabidopsis cuticular wax, was identified in both the ER-rich and the control mitochondria-enriched membrane fractions (Supplemental Fig. S5). This suggests that when tissue is homogenized and the lipid-rich cuticle is disrupted, surface waxes partition nonspecifically into multiple cellular membranes. These results indicate the potential pitfalls of using subcellular fractionation to study cuticular lipids in endomembrane compartments of cells.

The Secretory Mutants *gnl1-1* and *ech* Are Also Defective in Wax Biosynthesis

Whole ground stems of both *gnl1-1* and *ech* mutants contained significantly less total wax than wild-type stems (12 μg cm^{-2} for *gnl1-1* and 6 μg cm^{-2} for *ech* compared with 20 μg cm^{-2} for the wild type; Table I). These data suggest that while *ech* and *gnl1-1* are defective in wax secretion, they are also defective in wax biosynthesis. Interestingly, *rhd3-1* mutants, which are defective in ER morphology but not secretion (Chen et al., 2011), also contained significantly less total wax than the wild type (12 μg cm^{-2}; Table I; Supplemental Table S1).

Consistent with the decrease in wax biosynthesis in *rhd3-1*, *gnl1-1*, and *ech* mutants, there was no significant accumulation of waxes inside cells, as assayed by Nile red staining (Supplemental Fig. S4). *ech* mutant cells occasionally displayed large aggregations that stained with Nile red. However, these aggregations were extracellular, as defined by yellow fluorescent protein (YFP)-ABCG11 labeling of the plasma membrane (Supplemental Fig. S4C). These aggregations also label with toluidine blue and FM4-64, implying that they may not be composed exclusively of wax. Given the strong decrease in total wax biosynthesis in *rhd3-1*, *gnl1-1*, and *ech* mutants, it is unsurprising that retained intracellular waxes do not significantly aggregate within these cells, despite the secretion defects of these mutants.

It is possible that the decrease in wax synthesis in *rhd3-1*, *gnl1-1*, and *ech* mutants is due to a down-regulation or a mislocalization of the wax synthesis enzymes. To address this first hypothesis, transcript levels of wax synthesis enzymes were monitored in wild-type and mutant stems. No drastic changes were observed in transcript levels of several key wax biosynthesis genes in *rhd3-1*, *trs120-4*, *gnl1-1*, or *ech* stems relative to the wild type (Supplemental Fig. S6), suggesting that there was no negative feedback at the transcript level to regulate wax synthesis in these mutants. Because the largest decreases were observed for lipids longer than C26, the localization of one of the

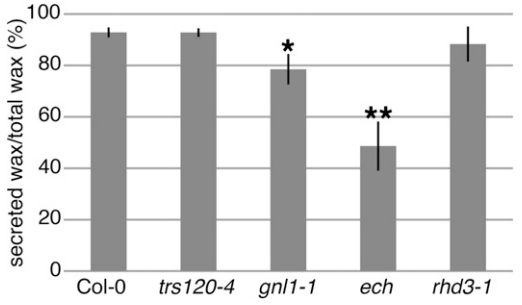

Figure 4. Vesicle transport mutants *ech* and *gnl1-1* are defective in wax secretion. The amount of secreted wax extracted by a short chloroform dip is expressed as a percentage of the total amount of wax extracted from homogenized stems; that is, secreted waxes are represented as a proportion of the total waxes synthesized. Significantly less wax was secreted in *gnl1-1* and *ech*. Values are means of three experiments of three biological replicates each (i.e. $n = 9$); error bars represent SE, and asterisks indicate statistically significant differences between wild-type and mutant wax secretion (Student's *t* test, $^{*}P < 0.05$, $^{**}P < 0.01$).

proteins required for fatty acid elongation, CER2-GFP (Haslam et al., 2012), was examined in the complemented *cer2-5* mutant and in *gnl1-1* and *ech*. In *cer2-5* complemented with *CER2pro*::*CER2-GFP*, the fluorescently tagged enzyme was detected at ER membranes, with some signal in the cytoplasm and nucleus, as reported by Haslam et al. (2012). While CER2-GFP was also localized to the ER network in both *gnl1-1* and *ech*, surprisingly, GFP label was also detected in endomembrane aggregations (Supplemental Fig. S7). Together, these data indicate that the wax biosynthesis defects in *gnl1-1* and *ech* are not due to changes in transcript levels or localization of the biosynthetic enzymes.

Defects in ER Morphology Are Correlated with Wax Biosynthesis Defects

Previous studies of *gnl1* and *ech* mutants have revealed altered ER morphology (Nakano et al., 2009; McFarlane et al., 2013), similar to the localization pattern of the ER membrane-localized CER2-GFP in *gnl1-1* and *ech* (Supplemental Fig. S7). Because waxes are synthesized by ER-localized enzymes, the wax biosynthesis defect in *rhd3-1*, *gnl1-1*, and *ech* mutants may be related to these defects in ER organization. Confocal microscopy of the ER lumen marker GFP-HDEL was used to assess ER morphology in *rhd3-1*, *gnl1-1*, and *ech*. These ER morphology data can be modeled as a surface rendering of the GFP-HDEL signal, which provides an overview of the ER within a cell (Fig. 5A), or single optical sections in confocal microscopy (Supplemental Fig. S8). In wild-type stem epidermal cells, GFP-HDEL labeled the web-like cortical ER network, transvacuolar strands, and perinuclear ER. In *rhd3-1*, most of the GFP-HDEL aggregated into thick, cable-like filaments in the center of the cell, as reported previously (Chen et al., 2011). In *ech* and *gnl1-1*, GFP-HDEL signal formed aggregates distributed throughout the cytosol (Fig. 5; Supplemental Fig. S8). *ech* stem epidermal cells contained large, very bright fluorescent aggregates that were saturated under conditions used to image wild-type ER (Fig. 5). Some internal membrane structure could be seen in these *ech* aggregates when the exposure time and detector gain were reduced (Supplemental Fig. S8). Aggregates of ER in *gnl1-1* mutants formed smaller, solid puncta when visualized with the ER lumen marker GFP-HDEL (Fig. 5; Supplemental Fig. S8), but no internal fluorescence was detected in these structures when CER2-GFP was used as an ER membrane marker (Supplemental Fig. S7), suggesting that these aggregates represent dilations of ER membranes in *gnl1-1* mutants.

To analyze the ER morphology of mutants and the wild type at high resolution, epidermal stem cells were cryofixed (high-pressure frozen and freeze substituted) and examined by transmission electron microscopy (TEM). In the wild type, tubular ER was largely confined to the peripheral cytoplasm. In *rhd3-1*, *gnl1-1*, and *ech* mutants, dilations of the ER were observed that had ribosomes on their cytoplasmic surface (Fig. 5). Some of these dilations resemble ER fusiform bodies that are commonly observed in Arabidopsis hypocotyl, leaf, and root cells. However, fusiform bodies were not observed in confocal microscopy or TEM of wild-type stem epidermal cells (Fig. 5; Supplemental Figs. S7 and S8). In contrast to *rhd3-1*, *gnl1-1*, and *ech* mutants, *trs120-4* mutants, which have wild-type wax load by GC-FID, displayed no ER morphology defects (Fig. 5).

To test whether ER morphology defects, independent of vesicle-trafficking phenotypes, affect wax biosynthesis, wax levels were assayed in the ER morphology mutant *rhd3-1*. This mutant provides a control in which ER morphology is disrupted, with no effect on secretion. GC-FID indicated that *rhd3-1* mutants also had

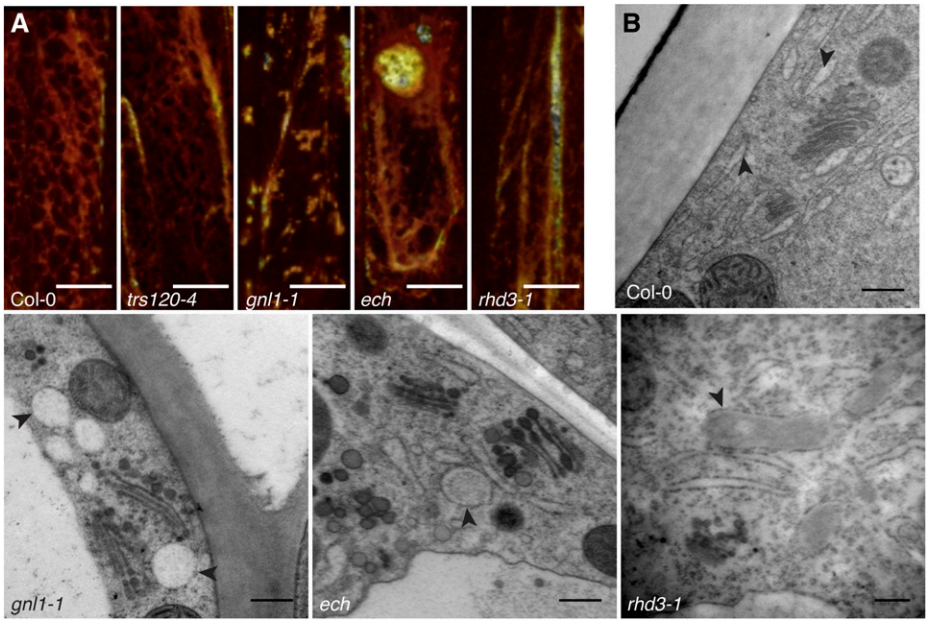

Figure 5. *gnl1-1*, *ech*, and *rhd3-1* are defective in ER morphology. A, In wild-type and *trs120-4* stem epidermal cells, the ER marker GFP-HDEL is localized primarily to a reticulate cortical network, as shown by three-dimensional surface rendering of the ER network in a single stem epidermal cell, while *gnl1-1*, *ech*, and *rhd3-1* mutants have defects in GFP-HDEL distribution. B, TEM reveals large dilations of the ER in *gnl1-1*, *ech*, and *rhd3-1* mutants relative to the tubular network observed in wild-type cells. Arrowheads point to the ER. Bars = 10 μm in A and 200 nm in B.

lower wax levels than the wild type (Fig. 6; Table I; Supplemental Table S1). Thus, the *rhd3-1* mutant provides another example of the correlation between mutants with defects in ER morphology and defects in wax biosynthesis. Furthermore, in the case of *rhd3*, the wax biosynthesis and ER morphology defects are independent of any defects in wax secretion.

DISCUSSION

Previously, the mechanism(s) of cuticular lipid traffic inside epidermal cells remained completely undefined, due to difficulties in studying intracellular lipid localization and trafficking. Isolation of endomembranes and mass spectroscopy confirmed that waxes are localized in the membranes of the cell, but further resolution within organelle subfractions was not possible because the hydrophobic surface waxes partitioned into multiple endomembrane fractions upon cell homogenization. Inhibitor studies are equally inappropriate for this system because of the difficulties in feeding inhibitors through the protective cuticle to stem epidermal cells. In order to examine the mechanism of cuticular wax secretion from the ER to the cell surface, we investigated wax secretion by employing a targeted genetic approach using an array of vesicle-trafficking and ER morphology mutants and quantitative chemical phenotyping. These data indicate that vesicle trafficking is required for intracellular wax traffic and raise a number of testable hypotheses for future research. Furthermore, these mutants revealed a relationship between the structure of the ER and its biosynthetic capacity.

The glossy phenotype and decreased wax load in *gnl1-1* and *ech* mutants can be attributed to the combination of less wax being produced, due to alterations in ER morphology, and disrupted vesicle traffic. In *gnl1-1* and *ech* cells, the proportion of wax that was successfully secreted to the cell surface was significantly lower than in the wild type, indicating that these mutants are defective in wax secretion. The wax secretion defect in *gnl1-1* mutants implies that vesicle trafficking between the ER and the cis-Golgi apparatus plays a key role in wax secretion to the cell surface, as GNL1 is an ADP-ribosylation factor guanine nucleotide-exchange factor required for COPI vesicle trafficking from the Golgi to the ER (Richter et al., 2007; Teh and Moore, 2007). Recent reports indicate that GNL1-mediated vesicle trafficking between the Golgi and the ER is particularly required for Golgi integrity and secretion during active epidermal cell expansion (Du et al., 2013), exactly when wax is synthesized and secreted (Suh et al., 2005). The *ech* mutant had the strongest wax secretion phenotype, suggesting that post-TGN vesicle traffic is also required for wax secretion. In contrast, the *rhd3-1* mutant, while suffering ER morphology defects and deficient wax biosynthesis, was not affected in wax secretion.

Interestingly, two different mutations in TGN-localized complexes downstream of *gnl1-1* at the Golgi resulted in different wax phenotypes: while *ech* mutants were defective in both wax synthesis and secretion, *trs120-4* mutants were able to synthesize and secrete wild-type levels of wax. These results may reflect the paradoxical nature of plant vesicle transport mutants; since mutations in key genes result in lethal or severely developmentally impaired phenotypes, weak alleles are required to study processes in mature plants, such as cuticular wax export, and residual gene activity in these weak alleles, such as *trs120-4*, might mask phenotypes. Alternatively, since the defects in *trs120-4* were severe enough to lead to changes in sec-GFP localization (Qi et al., 2011; Supplemental Fig. S1), wax secretion may be ECH dependent but TRS120 independent. This is consistent with emerging models of the plant TGN as a complex, multifunctional organelle from which many pathways in the endomembrane system diverge, including secretion to the plasma membrane/cell wall, secretion to the vacuole, endocytic recycling, and multivesicular body formation (Viotti et al., 2010; Scheuring et al., 2011). It is possible that two TGN-localized protein complexes may have completely different roles at the TGN. In support of this, VHA-a1, a TGN-localized vacuolar type H^+-ATPase, is mislocalized in *ech* (Gendre et al., 2011; Boutté et al., 2013) but not in *trs120* (Qi et al., 2011). Furthermore, the ECH complex is specifically required for secretion to the plasma membrane and cell wall but not for trafficking to the vacuole or recycling via the TGN/early endosome compartment (Gendre et al., 2013; Boutté et al., 2013). In contrast, the TRAPP II complex is required for trafficking to the cell wall and the cell plate, but it is not involved in recycling via the

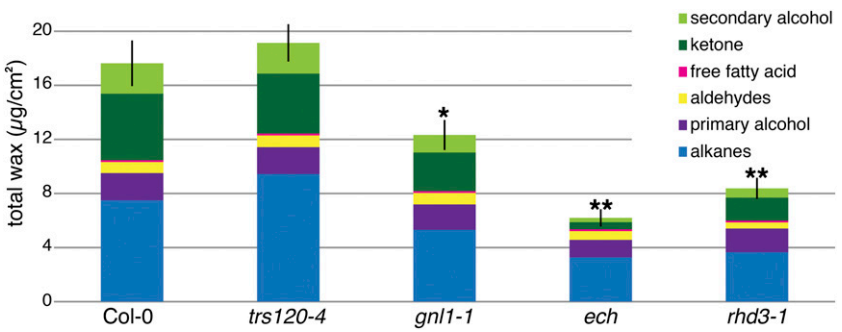

Figure 6. *gnl1-1*, *ech*, and *rhd3-1* are defective in wax biosynthesis. Quantification of total waxes, including intracellular and cuticular waxes, from ground stems via GC-FID reveals that *gnl1-1*, *ech*, and *rhd3-1*, but not *trs120-4*, mutants synthesize significantly less total wax than the wild type. Values are means of three experiments of three biological replicates each (i.e. $n = 9$); error bars represent SE of total wax load, and asterisks indicate statistically significant differences between wild-type and mutant total waxes (Student's *t* test, $*P < 0.05$, $**P < 0.01$).

TGN/early endosome, and its role in TGN-to-vacuole trafficking has not been assessed (Thellmann et al., 2010; Qi et al., 2011). Thus, the ECH complex and the TRAPP II complex may play distinct roles at the TGN, including different roles in wax secretion.

ER Structure Is Correlated with Its Biosynthetic Capacity

Three-dimensional surface rendering of the ER network using fluorescent markers for both the ER membrane and the ER lumen, and TEM, all demonstrated that ER morphology is disrupted in *rhd3-1*, *gnl1-1*, and *ech* mutants, while GC-FID of stem waxes indicated that these mutants all had reduced wax biosynthesis. Because waxes are synthesized by ER-localized enzymes, it is possible that this reduction in wax biosynthesis occurs as a direct result of ER disorganization. The fine-scale organization of enzymes in subcellular compartments can have important consequences for metabolism (for review, see Sweetlove and Fernie, 2013). Previous studies of heterologously expressed enzymes for lipid droplet synthesis, which also occurs primarily via ER-bound enzymes, have implied that these enzymes might organize within ER membranes to form enzyme clusters in specific subdomains of the ER, which would allow for metabolic channeling (Shockey et al., 2006; Gidda et al., 2011). A similar model has been proposed for wax biosynthesis: the immunophilin-like protein PASTICCINO1 (PAS1) is capable of interacting with all of the core components of the elongase complex and may serve as a scaffold for this multiprotein complex (Roudier et al., 2010).

Correlations of altered ER morphology and biosynthesis have also been described in *glutathione synthase* mutants (Au et al., 2012), where glutathione precursors accumulated in the ER, leading to morphological defects. Since Nile red staining of *gnl1-1* and *ech* revealed no significant lipid accumulation inside these mutants, the ER morphology defects are primary defects of the vesicle-trafficking phenotypes, not the result of wax accumulation. Similarly, in *abcg* transporter mutants that accumulate waxes in the ER, wax biosynthesis is unaffected (Pighin et al., 2004; McFarlane et al., 2010).

New Working Models of Intracellular Wax Trafficking

While these results have determined that cuticular lipid secretion in Arabidopsis requires vesicle trafficking, many questions about plant lipid trafficking remain. The requirement for vesicle trafficking during wax secretion could either be due to the direct delivery of wax components carried in the bilayer of the vesicles or to an indirect requirement for vesicle traffic delivering currently uncharacterized lipid export proteins. This study lays the groundwork for future research in plant lipid trafficking; further studies will be required to determine whether other components of the vesicle-trafficking machinery are active in wax export. For example, the hypothesis that wax molecules move in post-TGN vesicles suggests that the exocyst complex, which is involved in vesicle tethering to the plasma membrane, may also be required for lipid export. However, like the mutants in this study, it will be important to carefully select appropriate mutant alleles for study, since some exocyst complex mutants are seedling lethal and, therefore, do not produce stem epidermal lipids, while other mutants are extremely mild and, therefore, may not sufficiently disrupt vesicle trafficking (Zhang et al., 2010). Direct vesicle transport from the TGN to the plasma membrane would be predicted to be independent from the pathway leading to TGN maturation into multivesicular bodies recently described by Scheuring et al. (2011). It may also be that some of the *cer* mutants that remain uncharacterized could correspond to the secretory pathway machinery.

It also remains possible that some waxes reach the plant surface via a route that is independent of vesicle trafficking through the Golgi. By analogy with yeast and animal systems, some wax components may be transported via nonvesicular trafficking at ER-plasma membrane contact sites (Samuels and McFarlane, 2012). Indeed, several Arabidopsis proteins have shown nonvesicular lipid-trafficking capacity when expressed in yeast, although such a role in plants remains unclear (Pulsifer et al., 2012). The results described here do not exclude this possibility; because of the disruptions to ER morphology in the wax secretion-deficient mutants *gnl1-1* and *ech*, it is possible that some of the wax secretion defects may be due to the disorganization of ER-plasma membrane contact sites. However, because the proteins that mediate ER-plasma membrane contact in plants remain unknown, at present it is difficult to directly evaluate the role that these contact sites may play in lipid trafficking.

In summary, mutant analysis combined with live cell imaging, electron microscopy, and chemical phenotyping demonstrated that Arabidopsis waxes are transported from their site of synthesis in the ER to their site of accumulation on the plant surface via a mechanism that is dependent upon GNL1 at the Golgi apparatus and the ECH complex at the TGN. Furthermore, the disruption of ER morphology is correlated with decreased wax synthesis, suggesting a close relationship between the structure of the ER and its biosynthetic capacity. We propose a working model in which waxes are trafficked to the plasma membrane via GNL1- and ECH-dependent vesicle trafficking. Once in the plasma membrane, waxes must be extruded from the hydrophobic space in the bilayer via ABC transporters. Waxes would then be sequestered into the extracellular LTPs to traverse the hydrophilic cell wall and finally reach the cuticle, where they partition into the hydrophobic phase of the cuticle proper.

MATERIALS AND METHODS

Plant Material

Arabidopsis (*Arabidopsis thaliana*) seeds were sown on Arabidopsis medium plates and grown at 21°C, 70% to 80% humidity, and constant light

(approximately 100 μE m^{-2} s^{-1}) in an environmental growth chamber (Conviron). After 7 to 14 d, seedlings were transferred to Sunshine Mix 5 soil and returned to the same growth conditions. Plant lines were in the Columbia-0 (Col-0) background. All mutant lines were previously characterized and included the following: *ech* (ECH, At1g09330; Gendre et al., 2011), *abcg11-3* + *35S::YFP-ABCG11* (ABCG11, At1g17840; Bird et al., 2007), *abcg12-2* + *ABCG12pro::GFP-ABCG12* (ABCG12/CER5, At1g51500; Pighin et al., 2004), Col-0 + *35S::GFP-HDEL* and Col-0 + *35S::sec-GFP* (Batoko et al., 2000), *gnl1-1* (GNL1, At5g39500; Richter et al., 2007), *rhd3-1* (RHD3, At3g13870; Zheng et al., 2004), *trs120-4* (TRS120, At5g11040; Qi et al., 2011), and *cer2-5* + *CER2pro::CER2-GFP* (CER2, At4g24510; Haslam et al., 2012). All fluorescently tagged proteins (except secGFP and GFP-HDEL, which are markers) were maintained in the mutant background to avoid overexpression artifacts and/or complications between the tagged protein and the endogenous protein. Crosses were genotyped using transfer DNA-specific primers plus the primers indicated in Supplemental Table S2.

Preparation of Membrane Fractions

Microsomes and mitochondria were prepared from 7-d-old Arabidopsis seedlings grown in liquid Arabidopsis medium. Microsomes were isolated by homogenizing seedlings in 50 mM HEPES buffer (pH 7.6) with 400 mM Suc, 10 mM KCl, 3 mM EGTA, 3 mM Na-EDTA, 0.1% (w/v) fatty acid-free bovine serum albumin (Sigma), 1.5 mM dithiothreitol, and 1 mM sodium ascorbate, filtrating the homogenate through Miracloth (Calbiochem), centrifuging out large contaminants (6,000*g* for 15 min at 4°C), and centrifuging the supernatant at 60,000*g* for 30 min at 4°C.

Mitochondria were isolated based on a previously established procedure (http://www.edvotek.com/Plants). Briefly, 2 g of Arabidopsis seedlings was harvested and ground to a fine powder in liquid nitrogen. Then, the powder was mixed with 10 mL of cold lysis buffer (20 mM Tris-HCl, pH 7.4, 25% [v/v] glycerol, 20 mM KCl, 2 mM EDTA, 2.5 mM $MgCl_2$, 250 mM Suc, and 1 mM phenylmethylsulfonyl fluoride), and the homogenate was filtered through 95-μm and 40-μm nylon mesh sequentially. The flow through was spun at 4°C at 700*g* for 10 min to pellet the nuclei and cell debris. The supernatant was transferred and further centrifuged at 4°C at 10,000*g* for 10 min. The pellet at the bottom is enriched with intact mitochondria, which were washed using washing buffer (0.3 M Suc, 10 mM Tris, and 0.2% [w/v] bovine serum albumin) and centrifuged at 4°C at 10,000*g* for 10 min to obtain relatively pure mitochondria.

Mitochondrial and microsome fractions were resuspended in 10 mM HEPES buffer (pH 7.5) with 250 mM Suc and 20 mM KCl for further studies. Protein concentrations were determined using a Bradford assay kit (Bio-Rad).

Extraction and GC-MS Analysis of Membrane Lipids and Cuticular Waxes

The composition and quantity of fatty acids from membrane fractions were analyzed by GC-MS after direct acid-catalyzed transmethylation (Browse et al., 1986) with minor modification. Aliquots of membrane fractions were transmethylated in 5% (v/v) H_2SO_4 in methanol with 5 μg of 17:0 fatty acid methyl ester as an internal standard. Total fatty acid methyl esters were recovered in hexane extracts, dried under N_2, and redissolved in 100 μL of heptane. Samples were analyzed on a 30-m DB5-MS column by an Agilent 6850/5975 GC-MS apparatus run in scan mode (40–600 atomic mass units) with helium carrier gas (flow rate, 1.5 mL min^{-1}). The oven temperature program followed Haslam et al. (2012). Splitless injection was used, and peaks were quantified on the basis of their total ion current.

Cuticular wax was extracted from membrane fractions by chloroform with 100 ng of C24 alkane as an internal standard. The extract was dried under N_2, derivatized as below for GC-FID, and redissolved in 50 μL of toluene:heptane (1:1) for GC-MS analysis. Samples were analyzed by an Agilent 6890N/5975B GC-MS device on a 10-m DB5-MS column in scan mode (40–600 atomic mass units) with helium carrier gas (flow rate, 0.4 mL min^{-1}). The oven temperature program for wax analysis of microsome fractions followed Haslam et al. (2012) and for wax analysis of mitochondria fractions was set to 130°C for 3 min, increased to 320°C at 5°C min^{-1}, and held for an additional 10 min at 320°C. Splitless injection was used, and peaks were quantified on the basis of their total ion current.

GC-FID of Waxes

For surface waxes, samples were prepared as described by Haslam et al. (2012): 10-cm segments from 4- to 6-week-old stems were photographed and then immersed in HLPC-grade chloroform for 30 s, with 10 μg of 24-alkane as an internal standard. Extracted waxes were resuspended in 100 μL of chloroform, dried at 45°C under N_2, and resuspended in 10 μL of each pyridine (Sigma) and *N,O*-bis(trimethylsilyl) trifluoroacetamide with 1% trimethylchlorosilane (Sigma). Samples were derivatized at 75°C for 1 h, dried at 45°C under N_2, and resuspended in 50 μL of chloroform.

For total waxes (surface and intracellular), sample preparation and GC-FID were the same except that fresh stems were ground with 10 μg of 24-alkane as an internal standard and waxes were extracted from the homogenate by washing three times with chloroform. The washes were pooled, dried under nitrogen, derivatized, and resuspended as above.

Waxes were analyzed on an Agilent 7890A gas chromatograph coupled to a flame ionization detector with a 30-m by 320-μm HP-1 methyl siloxane column and hydrogen as the carrier gas; 1 μL of each sample was injected using a 2.7:1 split. The program was run at 50°C for 2 min, increased by 40°C min^{-1} to 200°C, held for 1 min at 200°C, increased by 3°C min^{-1} to 320°C, and held for 15 min at 320°C. Chromatogram peaks were identified by comparing their retention times with those of known standards. Because wax esters are very-low-abundance wax constituents of the Arabidopsis stem (Bird et al., 2007), they were difficult to detect in the wild type and often absent in *gnl1-1* and *ech*, so they were not included in further analyses. Total wax levels were determined by comparing the area of each peak with the 10-μg 24-alkane standard peak and then dividing by the surface area of the stem. Stem surface areas were measured by determining the area of the photographed stem in ImageJ and then multiplying by π. Means were calculated based on at least three independent experiments. Statistically significant differences between means were determined using Student's *t* test for each mutant compared with the wild type.

Confocal Microscopy

Stem segments from the first 3 cm below the shoot apical meristem (where wax synthesis and secretion is most active; Suh et al., 2005) were mounted in water and viewed using a Leica DMI6000 inverted microscope equipped with a Perkin-Elmer UltraView spinning-disk system and a Hamamatsu 9100-02 CCD camera. GFP was detected using a 488-nm laser and a 525/36-nm emission filter. YFP was detected using a 514-nm laser and a 540/30-nm emission filter. Nile red (Sigma; diluted 1:1,000 in water from a 1 mg mL^{-1} stock in dimethyl sulfoxide) and propidium iodide (Invitrogen; 1 μg mL^{-1} in water) were detected with a 561-nm laser and a 595/50-nm emission filter. Images were processed using ImageJ, and three-dimensional surface rendering of the ER was performed using Osirix (Rosset et al., 2004). Localization of YFP-ABCG11 was quantified by measuring normalized pixel intensity at three random cross sections in cells (in ImageJ) and by comparing internal signal with plasma membrane-localized signal. Statistically significant differences between means were determined using Student's *t* test for each mutant compared with the wild type.

Scanning Electron Microscopy

Mature stems were mounted on stubs in colloidal graphite Aquadag E (Canemco), frozen on liquid nitrogen, and transferred to the Emitech K1250 Cryo-System. Water was sublimed at −100°C for 30 min, then samples were viewed on a Hitachi S4700 field emission-scanning electron microscope at −130°C with an accelerating voltage of 5 kV, beam current of 10 μA, and working distance of 15 mm, using a mix of both the upper and lower detectors.

High-Pressure Freezing and TEM

TEM sample preparation, including high-pressure freezing, freeze-substitution sectioning, poststaining, and imaging, was performed as described by McFarlane et al. (2008). Briefly, stem segments from the first 3 cm below the shoot apical meristem (where wax synthesis and secretion is most active; Suh et al., 2005) were high-pressure frozen in B-type sample holders (Ted Pella) with 0.2 M Suc as a cryoprotectant using a Leica HPM-100. Samples were freeze substituted in 2% (w/v) osmium tetroxide and 8% (v/v) dimethoxypropane and infiltrated with Spurr's resin over 10 d. Samples were sectioned using a Leica Ultracut UCT and a Diatome diamond knife, mounted on copper grids (Gilder), and poststained with 2% (w/v) uranyl acetate in 70% (v/v) methanol and Reynolds' lead citrate. Samples were viewed using a

Hitachi H7600 TEM device at 80-kV accelerating voltage with an ATM Advantage CCD camera (Hamamatsu).

Gene Expression Analysis

Total RNA was extracted, using TRIzol reagent (Invitrogen), from stem segments 1 to 3 cm below the shoot apical meristem. Complementary DNA was synthesized from 5 μg of RNA using an oligo$(dT)_{18}$ primer and SuperScript III Reverse Transcriptase (Invitrogen). Reverse transcription-PCR was performed for 22 to 28 cycles using intron-flanking, gene-specific primers (Supplemental Table S2). Complementary DNA levels were normalized using primers for the *UBC10* ubiquitin-conjugating enzyme gene for 22 cycles.

Supplemental Data

The following materials are available in the online version of this article.

Supplemental Figure S1. *trs120-4*, *gnl1-1*, and *ech* are defective in secretion.

Supplemental Figure S2. ABCG12 is correctly localized to the plasma membrane in *gnl1-1* and *ech*.

Supplemental Figure S3. *gnl1-1* and *ech* wax accumulation phenotypes cannot be rescued by altering the chemical composition of surface waxes.

Supplemental Figure S4. Waxes do not substantially aggregate in *trs120-4*, *rhd3-1*, *gnl1-1*, or *ech* mutants.

Supplemental Figure S5. Waxes are associated with intracellular membranes.

Supplemental Figure S6. Transcript levels of wax biosynthetic genes are not affected in *gnl1-1*, *rhd3-1*, *ech*, or *trs120-4* mutants.

Supplemental Figure S7. The CER2 wax biosynthetic enzyme is localized to abnormal ER membranes in *gnl1-1* and *ech* mutants.

Supplemental Figure S8. *gnl1-1*, *ech*, and *rhd3-1* are defective in ER morphology.

Supplemental Table S1. Cuticular wax extracted from the plant surface compared to total stem wax in vesicle traffic mutants of Arabidopsis.

Supplemental Table S2. A list of primers employed in this study.

ACKNOWLEDGMENTS

We thank Ljerka Kunst, Xin Li, Mike Pollard, and Hugo Zheng for helpful discussions and comments on the manuscript and the University of British Columbia BioImaging Facility for technical assistance.

Received December 20, 2013; accepted January 16, 2014; published January 27, 2014.

LITERATURE CITED

Au KK, Pérez-Gómez J, Neto H, Müller C, Meyer AJ, Fricker MD, Moore I (2012) A perturbation in glutathione biosynthesis disrupts endoplasmic reticulum morphology and secretory membrane traffic in *Arabidopsis thaliana*. Plant J **71:** 881–894

Batoko H, Zheng HQ, Hawes C, Moore I (2000) A rab1 GTPase is required for transport between the endoplasmic reticulum and Golgi apparatus and for normal Golgi movement in plants. Plant Cell **12:** 2201–2218

Bernard A, Domergue F, Pascal S, Jetter R, Renne C, Faure JD, Haslam RP, Napier JA, Lessire R, Joubès J (2012) Reconstitution of plant alkane biosynthesis in yeast demonstrates that *Arabidopsis* ECERIFERUM1 and ECERIFERUM3 are core components of a very-long-chain alkane synthesis complex. Plant Cell **24:** 3106–3118

Bertho P, Moreau P, Morré DJ, Cassagne C (1991) Monensin blocks the transfer of very long chain fatty acid containing lipids to the plasma membrane of leek seedlings: evidence for lipid sorting based on fatty acyl chain length. Biochim Biophys Acta **1070:** 127–134

Bird D, Beisson F, Brigham A, Shin J, Greer S, Jetter R, Kunst L, Wu X, Yephremov A, Samuels L (2007) Characterization of Arabidopsis ABCG11/WBC11, an ATP binding cassette (ABC) transporter that is required for cuticular lipid secretion. Plant J **52:** 485–498

Boutté Y, Jonsson K, McFarlane HE, Johnson E, Gendre D, Swarup R, Friml J, Samuels L, Robert S, Bhalerao RP (2013) ECHIDNA-mediated post-Golgi trafficking of auxin carriers for differential cell elongation. Proc Natl Acad Sci USA **110:** 16259–16264

Browse J, McCourt PJ, Somerville CR (1986) Fatty acid composition of leaf lipids determined after combined digestion and fatty acid methyl ester formation from fresh tissue. Anal Biochem **152:** 141–145

Chen J, Stefano G, Brandizzi F, Zheng H (2011) Arabidopsis RHD3 mediates the generation of the tubular ER network and is required for Golgi distribution and motility in plant cells. J Cell Sci **124:** 2241–2252

Coll EP, Kandt C, Bird DA, Samuels AL, Tieleman DP (2007) The distribution and conformation of very long-chain plant wax components in a lipid bilayer. J Phys Chem B **111:** 8702–8704

DeBono A, Yeats TH, Rose JK, Bird DA, Jetter R, Kunst L, Samuels L (2009) *Arabidopsis* LTPG is a glycosylphosphatidylinositol-anchored lipid transfer protein required for export of lipids to the plant surface. Plant Cell **21:** 1230–1238

Du W, Tamura K, Stefano G, Brandizzi F (2013) The integrity of the plant Golgi apparatus depends on cell growth-controlled activity of GNL1. Mol Plant **6:** 905–915

Gendre D, McFarlane HE, Johnson E, Mouille G, Sjödin A, Oh J, Levesque-Tremblay G, Watanabe Y, Samuels L, Bhalerao RP (2013) Trans-Golgi network localized ECHIDNA/Ypt interacting protein complex is required for the secretion of cell wall polysaccharides in *Arabidopsis*. Plant Cell **25:** 2633–2646

Gendre D, Oh J, Boutté Y, Best JG, Samuels L, Nilsson R, Uemura T, Marchant A, Bennett MJ, Grebe M, et al (2011) Conserved Arabidopsis ECHIDNA protein mediates trans-Golgi-network trafficking and cell elongation. Proc Natl Acad Sci USA **108:** 8048–8053

Gidda SK, Shockey JM, Falcone M, Kim PK, Rothstein SJ, Andrews DW, Dyer JM, Mullen RT (2011) Hydrophobic-domain-dependent protein-protein interactions mediate the localization of GPAT enzymes to ER subdomains. Traffic **12:** 452–472

Greer S, Wen M, Bird DA, Wu X, Samuels L, Kunst L, Jetter R (2007) The cytochrome P450 enzyme CYP96A15 is the midchain alkane hydroxylase responsible for formation of secondary alcohols and ketones in stem cuticular wax of Arabidopsis. Plant Physiol **145:** 653–667

Haslam TM, Kunst L (2013) Extending the story of very-long-chain fatty acid elongation. Plant Sci **210:** 93–107

Haslam TM, Mañas-Fernández A, Zhao L, Kunst L (2012) Arabidopsis ECERIFERUM2 is a component of the fatty acid elongation machinery required for fatty acid extension to exceptional lengths. Plant Physiol **160:** 1164–1174

Kim H, Lee SB, Kim HJ, Min MK, Hwang I, Suh MC (2012) Characterization of glycosylphosphatidylinositol-anchored lipid transfer protein 2 (LTPG2) and overlapping function between LTPG/LTPG1 and LTPG2 in cuticular wax export or accumulation in Arabidopsis thaliana. Plant Cell Physiol **53:** 1391–1403

Koornneef M, Hanhart CJ, Thiel F (1989) A genetic and phenotypic description of *eceriferum* (*cer*) mutants in *Arabidopsis thaliana*. J Hered **80:** 118–122

Mansbach CM, Siddiqi SA (2010) The biogenesis of chylomicrons. Annu Rev Physiol **72:** 315–333

McFarlane HE, Shin JJ, Bird DA, Samuels AL (2010) *Arabidopsis* ABCG transporters, which are required for export of diverse cuticular lipids, dimerize in different combinations. Plant Cell **22:** 3066–3075

McFarlane HE, Watanabe Y, Gendre D, Carruthers K, Levesque-Tremblay G, Haughn GW, Bhalerao RP, Samuels L (2013) Cell wall polysaccharides are mislocalized to the vacuole in *echidna* mutants. Plant Cell Physiol **54:** 1867–1880

McFarlane HE, Young RE, Wasteneys GO, Samuels AL (2008) Cortical microtubules mark the mucilage secretion domain of the plasma membrane in Arabidopsis seed coat cells. Planta **227:** 1363–1375

Nakano RT, Matsushima R, Ueda H, Tamura K, Shimada T, Li L, Hayashi Y, Kondo M, Nishimura M, Hara-Nishimura I (2009) GNOM-LIKE1/ERMO1 and SEC24a/ERMO2 are required for maintenance of endoplasmic reticulum morphology in *Arabidopsis thaliana*. Plant Cell **21:** 3672–3685

Pighin JA, Zheng H, Balakshin LJ, Goodman IP, Western TL, Jetter R, Kunst L, Samuels AL (2004) Plant cuticular lipid export requires an ABC transporter. Science **306:** 702–704

Pollard M, Beisson F, Li Y, Ohlrogge JB (2008) Building lipid barriers: biosynthesis of cutin and suberin. Trends Plant Sci **13:** 236–246

Pulsifer IP, Kluge S, Rowland O (2012) Arabidopsis long-chain acyl-CoA synthetase 1 (LACS1), LACS2, and LACS3 facilitate fatty acid uptake in yeast. Plant Physiol Biochem **51:** 31–39

Qi X, Kaneda M, Chen J, Geitmann A, Zheng H (2011) A specific role for Arabidopsis TRAPPII in post-Golgi trafficking that is crucial for cytokinesis and cell polarity. Plant J **68:** 234–248

Richter S, Geldner N, Schrader J, Wolters H, Stierhof YD, Rios G, Koncz C, Robinson DG, Jürgens G (2007) Functional diversification of closely related ARF-GEFs in protein secretion and recycling. Nature **448:** 488–492

Robinson DG, Langhans M, Saint-Jore-Dupas C, Hawes C (2008) BFA effects are tissue and not just plant specific. Trends Plant Sci **13:** 405–408

Rosset A, Spadola L, Ratib O (2004) OsiriX: an open-source software for navigating in multidimensional DICOM images. J Digit Imaging **17:** 205–216

Roudier F, Gissot L, Beaudoin F, Haslam R, Michaelson L, Marion J, Molino D, Lima A, Bach L, Morin H, et al (2010) Very-long-chain fatty acids are involved in polar auxin transport and developmental patterning in *Arabidopsis*. Plant Cell **22:** 364–375

Rowland O, Zheng H, Hepworth SR, Lam P, Jetter R, Kunst L (2006) *CER4* encodes an alcohol-forming fatty acyl-coenzyme A reductase involved in cuticular wax production in Arabidopsis. Plant Physiol **142:** 866–877

Samuels L, Kunst L, Jetter R (2008) Sealing plant surfaces: cuticular wax formation by epidermal cells. Annu Rev Plant Biol **59:** 683–707

Samuels L, McFarlane HE (2012) Plant cell wall secretion and lipid traffic at membrane contact sites of the cell cortex. Protoplasma (Suppl 1) **249:** S19–S23

Scheuring D, Viotti C, Krüger F, Künzl F, Sturm S, Bubeck J, Hillmer S, Frigerio L, Robinson DG, Pimpl P, et al (2011) Multivesicular bodies mature from the trans-Golgi network/early endosome in *Arabidopsis*. Plant Cell **23:** 3463–3481

Shockey JM, Gidda SK, Chapital DC, Kuan JC, Dhanoa PK, Bland JM, Rothstein SJ, Mullen RT, Dyer JM (2006) Tung tree DGAT1 and DGAT2 have nonredundant functions in triacylglycerol biosynthesis and are localized to different subdomains of the endoplasmic reticulum. Plant Cell **18:** 2294–2313

Suh MC, Samuels AL, Jetter R, Kunst L, Pollard M, Ohlrogge J, Beisson F (2005) Cuticular lipid composition, surface structure, and gene expression in Arabidopsis stem epidermis. Plant Physiol **139:** 1649–1665

Sweetlove LJ, Fernie AR (2013) The spatial organization of metabolism within the plant cell. Annu Rev Plant Biol **64:** 723–746

Teh OK, Moore I (2007) An ARF-GEF acting at the Golgi and in selective endocytosis in polarized plant cells. Nature **448:** 493–496

Thellmann M, Rybak K, Thiele K, Wanner G, Assaad FF (2010) Tethering factors required for cytokinesis in Arabidopsis. Plant Physiol **154:** 720–732

Viotti C, Bubeck J, Stierhof YD, Krebs M, Langhans M, van den Berg W, van Dongen W, Richter S, Geldner N, Takano J, et al (2010) Endocytic and secretory traffic in *Arabidopsis* merge in the trans-Golgi network/early endosome, an independent and highly dynamic organelle. Plant Cell **22:** 1344–1357

Zhang GF, Driouich A, Staehelin LA (1993) Effect of monensin on plant Golgi: re-examination of the monensin-induced changes in cisternal architecture and functional activities of the Golgi apparatus of sycamore suspension-cultured cells. J Cell Sci **104:** 819–831

Zhang M, Wu F, Shi J, Zhu Y, Zhu Z, Gong Q, Hu J (2013) ROOT HAIR DEFECTIVE3 family of dynamin-like GTPases mediates homotypic endoplasmic reticulum fusion and is essential for Arabidopsis development. Plant Physiol **163:** 713–720

Zhang Y, Liu CM, Emons AM, Ketelaar T (2010) The plant exocyst. J Integr Plant Biol **52:** 138–146

Zheng H, Kunst L, Hawes C, Moore I (2004) A GFP-based assay reveals a role for RHD3 in transport between the endoplasmic reticulum and Golgi apparatus. Plant J **37:** 398–414